Critical Evaluation of Strong Ground Motions in Izmir and Implications for Future Earthquake Simulation Results

Şahin Çağlar Tuna

Department of Civil Engineering, Yaşar University, Izmir, Türkiye

ABSTRACT

Izmir, a major city in western Turkey, is located in a highly seismic region, subject to frequent earthquakes due to its proximity to active fault systems. This paper critically evaluates the strong ground motions recorded in Izmir, with a focus on understanding the implications for urban infrastructure and future seismic hazard mitigation. Historically available data is collected and compared with the available ground motion prediction equations (GMPE). Later, the most appropriate prediction equation is selected and used to determine the target response spectrum. 2020 Sisam earthquake is a well-documented seismic event and the data from the stations are then used to further calibrate the 1D site response model. Lastly, possible future events are generated and results are compared with the current Turkish Earthquake Code (TEC). Amplification factors prescribed by code for Izmir Bay have been surpassed by projected future events, highlighting the necessity for reassessment. Therefore, region-specific seismic zoning should be established when standard code practices fall short in accounting for significant site effects. Concrete recommendations about local site modification factors and evaluations on this topic have been provided within the article.

Keywords: Ground motion prediction equations, Site response, Future events, Local site modification factors

1. INTRODUCTION

Throughout history, Izmir—Turkey's third-largest city—has been repeatedly affected by destructive earthquakes due to its location near active fault systems along the Aegean coast. With its dense urban fabric and economic significance, understanding seismic hazard in the region is crucial for enhancing urban resilience and risk mitigation. The city is underlain by thick Quaternary alluvial deposits, which are known to significantly amplify incoming seismic waves, especially in deep basin areas. This amplification poses a serious threat to the built environment, particularly for buildings with fundamental periods resonating with the local site response.

The 2020 Samos earthquake provided a striking demonstration of these effects: in districts such as Bayraklı, field observations and numerical simulations showed that spectral accelerations in the 0.7–1.0 s period range exceeded Turkish Earthquake Code (TEC, 2018) predictions by factors of 4 to 6 (Cetin et al., 2022; Gülerce et al., 2022). These unexpected amplifications have been attributed to complex basin geometries, soft soil layers, and high impedance contrasts (Cetin et al., 2023). Such site-specific effects, which are not fully captured in conventional design spectra, highlight the urgent need for detailed ground motion characterization in Izmir

Although numerous studies have addressed local site effects or assessed GMPEs independently, most fall short of providing an integrated framework that unites strong-motion recordings, deterministic scenario modeling, and code-based spectrum comparison. This gap underscores the need for regionally calibrated GMPEs and basin-aware design spectra that can explicitly account for spatially variable amplification across Izmir Bay.Conventional site classification approaches, moreover, often fail to capture the spatial variability in seismic demand across basin environments like Izmir Bay.

This study bridges that gap by combining nearly three decades (1996–2024) of empirical strong-motion data with residual-based GMPE evaluations and site-specific response analyses using a validated DeepSoil model. By incorporating these elements into a unified simulation framework, the study highlights how code-based design spectra—when lacking localized amplification considerations—may significantly underestimate seismic demand in urban basins. The proposed methodology thus offers a regionally calibrated and practically transferable foundation for performance-based seismic design in Izmir and similar tectonic settings.

The purpose of this study is divided into two main parts: First part is to evaluate the strong ground motions recorded in Izmir during past seismic events, particularly focusing on their effects on local geotechnical conditions and built environments. In the second part, a future earthquake scenario and potential engineering outcomes will be examined by using the findings obtained in the first part.

To achieve these goals, the study follows a structured methodology comprising the following steps:

a. Data Collection: Gathering historical earthquake data from the Izmir region, including earthquake magnitudes, source-to-site distances, and PGA measurements.
b. Selection of GMPEs: Choosing GMPE models that are applicable to the regional tectonic and geological conditions.

c. Comparison of GMPE Predictions and evaluation of GMPE Accuracy: Comparing the predicted PGA values from different GMPEs with the observed values from historical earthquakes. Differences were observed between the predicted and actual ground motions, emphasizing the importance of site-specific adjustments in GMPEs for accurate seismic hazard assessment. Using statistical methods, such as Root Mean Square Error (RMSE), to assess the accuracy of the GMPE predictions and identify the most reliable model for the Izmir region. Apply necessary improvements for the prediction equations to comply with the specific directivity and near fault effects.
d. 1D site response analysis were firstly validated with the available recordings and then set up for the future earthquake scenarios.
e. Developing target spectra using the outcomes of 3rd step, evaluating future earthquakes in the region and comparison with the current TEC results.
f. The study concludes with recommendations on refining seismic hazard models to account for local site effects and improving the predictive accuracy of GMPEs in areas with complex soil profiles. These findings have implications for earthquake-resistant design and site-specific seismic risk mitigation strategies.

By integrating a comprehensive set of strong-motion recordings, residual-based GMPE evaluation, and site-specific response analysis within a deterministic simulation framework, this study establishes a regionally calibrated seismic design basis for Izmir. The methodology not only captures basin-induced amplification effects often overlooked by code-based spectra but also provides a transferable approach for seismic hazard assessment in other urban basins with similar geological and tectonic settings.

1.1. Regional Seismicity and Geological Settings of Izmir Bay

Izmir is located in the western part of Turkey, within the tectonically active Aegean Extensional Province. This region is characterized by widespread normal faulting, primarily driven by back-arc extension associated with the subduction of the African Plate beneath the Eurasian Plate along the Hellenic Trench (McKenzie, 1978). Historically, the region has experienced several destructive earthquakes, most notably the 1688 and 1778 events, which caused widespread structural damage and loss of life in the Izmir area (Tepe et al., 2021). The ongoing crustal extension has resulted in crustal thinning, frequent shallow-focus earthquakes, and persistent seismicity throughout Western Anatolia (Emre et al., 2005).

The seismotectonic framework of the region includes a complex network of both normal and strike-slip faults. These structures, many of which are segmented and capable of multi-segment ruptures, are comprehensively documented in the GIS-based Active Fault Database of Turkey (Emre et al., 2018). This database provides detailed information on fault activity classifications, geometries, and slip rates essential for seismic hazard assessments. The Izmir metropolitan area lies in close proximity to several active fault zones, as illustrated in Figure 1, underscoring the city's exposure to significant seismogenic sources.

In addition to this tectonic complexity, the Izmir Bay region is underlain by thick accumulations of Quaternary alluvial and sedimentary deposits. These geologic conditions contribute to pronounced site-specific amplification

effects, especially in soft soil basins where seismic waves may be significantly intensified. Consequently, the combined influence of active faulting and local geology necessitates detailed ground motion characterization and site response analysis for reliable seismic risk assessment (Ocakoğlu et al., 2005; Akyol et al., 2006).

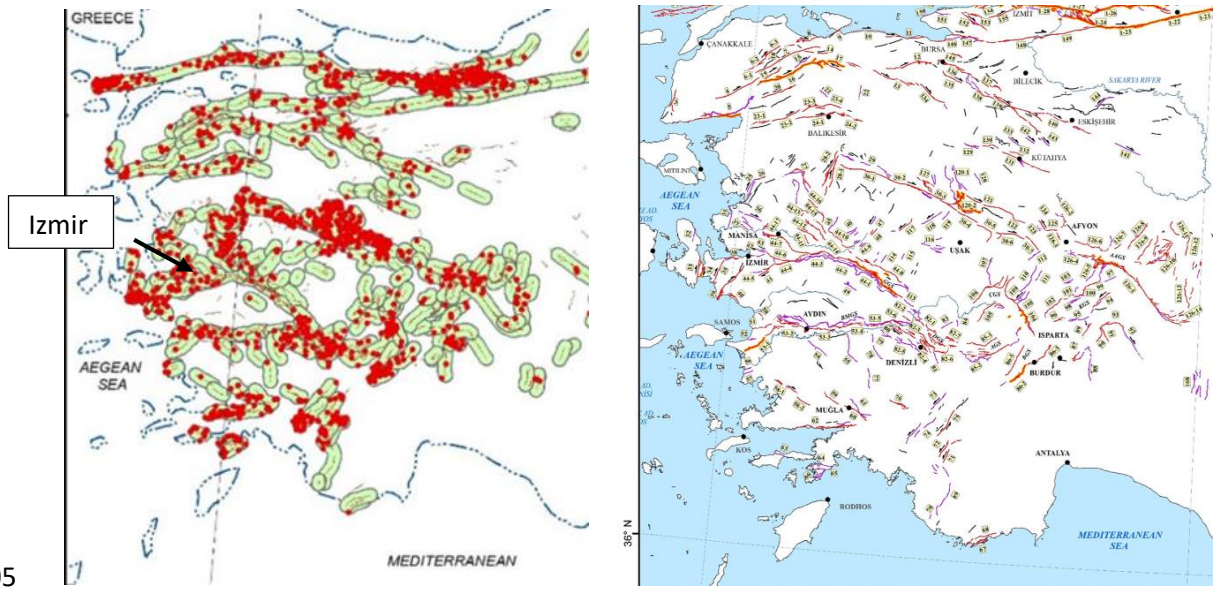

Figure 1. Active Seismic Faults and recent earthquakes in the region (Emre et.al, 2018)

The geological framework of Izmir is markedly heterogeneous, comprising a combination of sedimentary basins, alluvial plains, and sporadic rock outcrops. These spatially variable ground conditions play a pivotal role in modulating seismic wave propagation, particularly through amplification mechanisms driven by soft soil layers and impedance contrasts. This phenomenon is especially pronounced in areas where unconsolidated sediments dominate the subsurface, resulting in significant variations in shaking intensity and spectral content during earthquakes.

A regional geological map illustrating the distribution of major lithological units and active fault lines is presented in Figure 2. The map clearly delineates the extent of alluvial plains and the underlying bedrock zones, offering critical insight into potential site response variations across the study area.

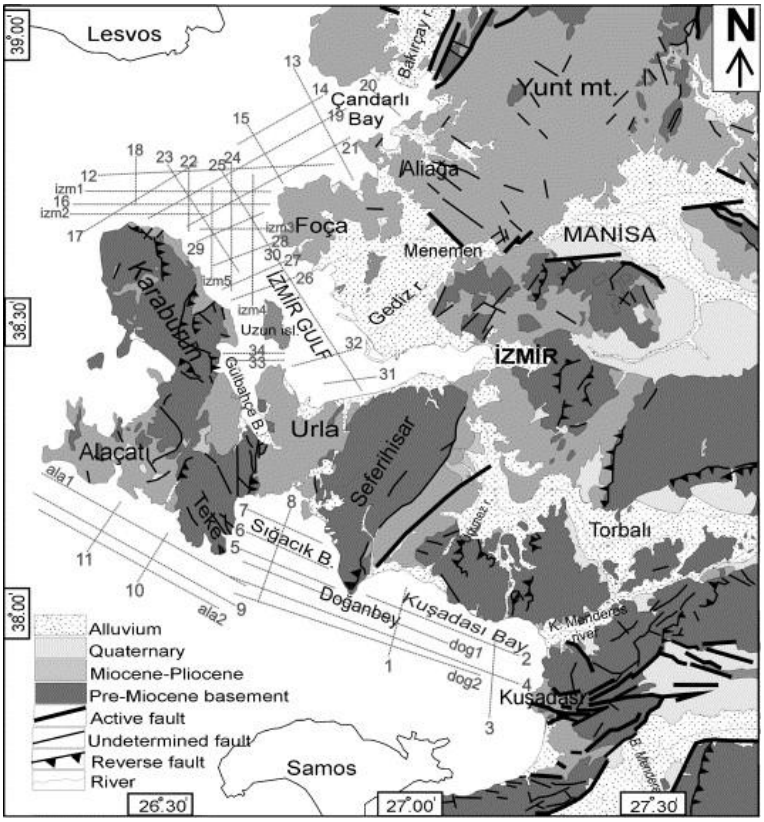

Figure 2. Geology map of the study area and location of the seismic fault lines (Adapted from Ocakoglu et.al, 2005).

The Izmir Bay region includes several structurally controlled sedimentary basins such as the Gediz Graben and margins of the Menderes Massif. These basins are filled with geologically young, unconsolidated sediments that are highly susceptible to seismic wave amplification. Much of the coastal zone, particularly surrounding the bay, is composed of loose alluvial deposits with low stiffness and high porosity. These characteristics are known to significantly enhance ground motion amplitudes and contribute to localized damage concentration during seismic events.

2. Compilation of the strong motion dataset and predictive performance of current ground motion models

Ground Motion Prediction Equations (GMPEs) are empirical or semi-empirical formulations developed to estimate expected ground motion parameters—such as peak ground acceleration (PGA)—at a given site, based on variables including earthquake magnitude, source-to-site distance, and local site conditions (Gülerce et al., 2022). These models are fundamental tools in probabilistic seismic hazard analysis (PSHA) and performance-based earthquake engineering.

Given the seismically active nature of the Western Anatolian region and the complex geological and tectonic characteristics of Izmir, selecting a regionally appropriate and predictively reliable GMPE is critical. Various models have been proposed for different tectonic environments; for instance, the Euro-Mediterranean region is

well-represented by the NGA-Europe models developed by Akkar and Bommer (2010) and Akkar et al. (2014). In Turkey, Kalkan and Gülkan (2004) introduced a site-dependent GMPE based on national datasets. However, many of these models exhibit limitations, including restricted magnitude–distance ranges, insufficient treatment of site-specific effects, or limited representation of near-fault ground motions.

In this study, eight GMPEs from the NGA-West1 and NGA-West2 projects were selected due to their methodological robustness, comprehensive magnitude–distance coverage, and well-established site adjustment formulations based on Vs30. Models such as Boore et al. (2014) and Chiou and Youngs (2014) were included, owing to their wide adoption in international hazard frameworks and their applicability to site-specific studies in urban basins like Izmir.

To evaluate their predictive performance, a strong-motion dataset comprising 33 earthquake records from 1996 to 2024 was compiled from the Turkish Disaster and Emergency Management Presidency (AFAD). These events span a broad spectrum of moment magnitudes (Mw) and source-to-site distances, thus enabling a robust assessment of model performance across varying seismic scenarios (Table 1).

All records were obtained from two well-instrumented stations located in the Bornova district: Station 3502 (Vs30 = 270 m/s) and Station 3522 (Vs30 = 249 m/s), both corresponding to NEHRP Site Class D (FEMA, 2001) conditions. The use of two stations with similar geotechnical classifications helps minimize variability from local soil conditions and enhances the comparability of model outputs, making the findings particularly relevant to the soft-soil conditions prevalent in much of urban Izmir.

Despite the regional relevance and methodological consistency of the selected GMPEs, several epistemic uncertainties persist. These stem from potential regional discrepancies in model calibration, simplified rupture-to-site distance metrics, and the scarcity of near-fault recordings within the compiled historical dataset. Moreover, although both recording stations are categorized as NEHRP Site Class D (FEMA, 2001), subtle variations in subsurface stratigraphy and nonlinear site response characteristics may not be fully captured through Vs30-based adjustments alone. These limitations highlight the need for ongoing regional calibration efforts and the integration of high-resolution geotechnical and seismic data to improve ground motion modeling accuracy in complex urban basins such as Izmir.

The predicted peak ground acceleration (PGA) values from each GMPE were then compared with the observed PGA values from the 33 historical records. The comparison results are summarized in Figure 3, while Table 2 provides a list of the selected GMPEs.

Table 1.Important characteristics of the historical seismic events

Event No	Event Name	Mw	Epicentral Distance - km	Fault Mechanism	Event Depth -km	PGA Max - cm/s2
1	2.04.1996	4.9	71.81	Normal	12	18.42
2	14.11.1997 Aegean Sea (Kusadası)	5.8	128.79	Normal	12	6.03
3	09.07.1998 Aegean Sea	5	75.48	Normal	12.5	27.06
4	22.01.1999 Buca-İzmir	3.4	9.95	Strike Slip	5	2.985
5	17.08.1999 Golcuk (Izmit)	7.6	346.5	Strike Slip	15.9	10.8
6	21.01.2002 Turgutlu (Manisa)	4.8	60.11	Normal	11.7	6.981
7	10.04.2003 - Seferihisar	5.7	37.45	Strike Slip	18.7	78.57
8	17.04.2003 Seferihisar (Izmir)	5.2	61.55	Strike Slip	11.5	8.851
9	29.01.2005	4.9	47.67	Normal	20	6.131
10	17.10.2005 - Urla	5.8	58.21	Strike Slip	11	13.12
11	17.10.2005 - Urla	5.4	56.17	Strike Slip	20.5	16.51
12	20.10.2005 - Urla	5.9	58.98	Strike Slip	15.4	31.773
13	24.12.2005 Akhisar (Manisa)	4.9	64.85	Normal	6	3.14
14	19.05.2011 Simav (Kutahya)	5.7	180.7	Normal	24.46	5.533
15	8.01.2013 - Aegean Sea	6.2	194		26.83	3.642
16	24.05.2014 - Aegean Sea	6.5	255.78		25	7.659
17	19.07.2014 - Konak- İzmir	3.7	10	Strike Slip	6.98	9.47
18	02.06.2017 Ayvacik (Canakkale)	5.3	154.13	Normal	14.16	1.466
19	12.06.2017-Karaburun	6.2	43.87	Normal	15.86	58.306
20	12.06.2017-Karaburun	6.2	89.62	Normal	15.86	25.499
21	17.06.2017 Aegean Sea	5.3	81.15	Normal	9.11	9.42
22	20.07.2017 Aegean Sea(Bodrum)	6.5	169.93	Normal	19.44	4.44
23	08.08.2019 Bozkurt (Denizli)	6	218.49	Normal	10.92	0.39
24	18.02.2020 Kırkağaç (Manisa)	5.2	91.02	Normal	6.98	4.662
25	26.06.2020- Saruhanlı-Manisa	5.5	64.1	Normal	9.29	7.109
26	28.06.2020 Ege Denizi (Mugla)	5.2	214.57	Normal	61.42	3.375
27	30.10.2020 Sisam	5.1	72.95	Normal	7.71	7.056
28	30.10.2020- Sisam	7	75.57	Normal	16.54	73.72
29	21.04.2021-Sehzadeler-Manisa	4.9	40.19	Normal	13.2	9.673
30	21.06.2021 Aegean Sea (Datca)	5.3	228.34	Normal	14.74	0.61
31	11.04.2022- Buca - İzmir	4.9	9.81	Strike Slip	14.47	48.59
32	01.10.2023 Lesvos	5	130.95	Normal	14.95	1.708
33	27.01.2024 Aegean Sea (Kusadası)	5.1	52.46	Normal	8.51	7.632

Table 2. GMPEs Used In this Study

No	Ground Motion Prediction Equation
1	AS08: Abrahamson & Silva (2008) NGA Model
2	BA08: Boore & Atkinson (2008) NGA Model
3	CB08: Campbell & Bozorgnia (2008) NGA Model
4	CY08: Chiou & Youngs (2008) NGA Model
5	ASK14: Abrahamson, Silva & Kamai (2014) NGA-West2 Model
6	BSSA14: Boore, Stewart, Seyhan & Atkinson (2014) NGA-West2 Model
7	CB14: Campbell & Bozorgnia (2014) NGA-West2 Model
8	CY14: Chiou & Youngs (2014) NGA-West2 Model

To quantify the predictive accuracy of the selected GMPEs, statistical error analyses were conducted using two commonly employed metrics: the Root Mean Square Error (RMSE) and the Coefficient of Determination (R^2). These metrics aim to assess which GMPE most accurately captures the observed peak ground accelerations (PGA) across a range of earthquake magnitudes and site conditions. The comparative results are presented in Table 3.

RMSE is widely used to evaluate the deviation between observed and predicted values. It is particularly sensitive to large errors, thereby emphasizing models that perform consistently across the dataset. The RMSE is defined as:

$$\text{RMSE} = \sqrt{\frac{1}{N}\sum_{i=1}^{N}(PGA_{observed,i} - PGA_{predicted,i})^2} \quad (1)$$

Where:

- N is the number of the earthquake records
- i is the index of each event,
- $PGA_{observed,i}$ is the observed PGA for the i-th earthquake
- $PGA_{predicted,i}$ is the predicted PGA for the i-th earthquake based on the GMPE.

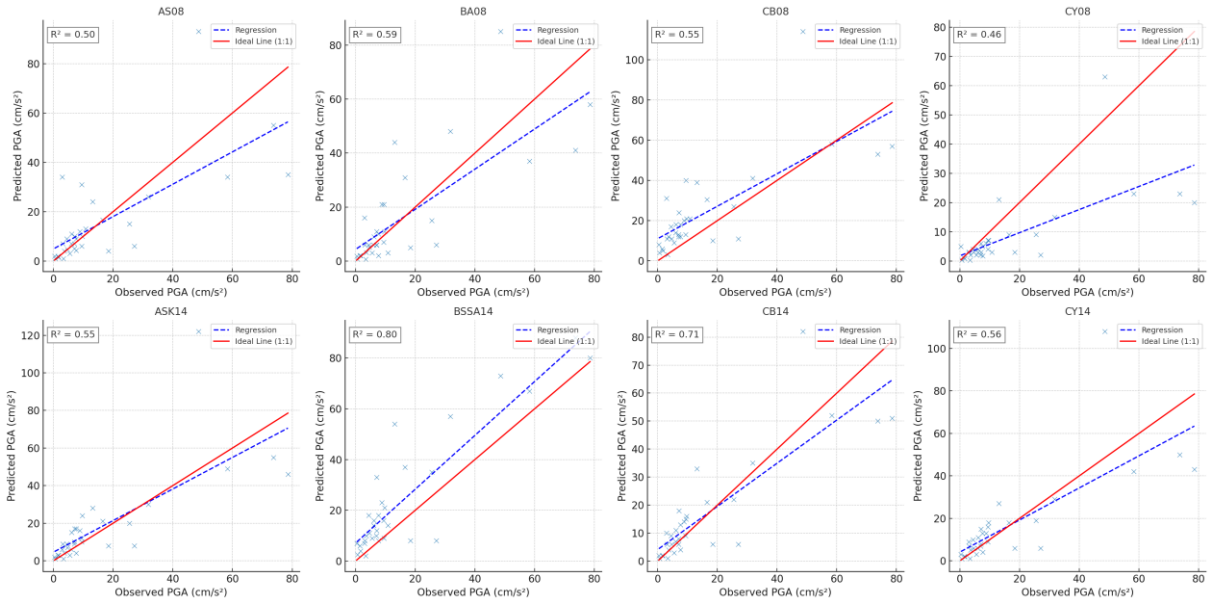

Figure 3. Scatter plots comparing observed and predicted PGA values for eight GMPEs. (The 1:1 line (red) represents perfect prediction, while the regression line (blue, dashed) and R^2 values indicate model-specific fit quality.)

To interpret the predictive capacity of each GMPE, scatter plots comparing observed versus predicted PGA values were generated for all eight models (Figure 3). The 1:1 reference line denotes perfect prediction, while deviations from this line indicate systematic bias or dispersion. A variety of factors contribute to discrepancies among the models, including site-specific amplification effects, differences in magnitude–distance scaling, depth parameterization, and the internal constants adopted by each model.

Since isolating these effects is not feasible with the available dataset, the analysis relies on statistical performance metrics—specifically R^2 and RMSE—to rank the models. Based on these results (Table 3), CB14 and BSSA14 emerged as the most accurate and consistent predictors, demonstrating the highest R^2 (0.71 and 0.80, respectively) and lowest RMSE values (11.03 and 13.39 cm/s², respectively).

Table 3. Result of GMPE Error Analysis

GMPE	R^2	RMSE (cm/s²)
AS08	0.5	14.85
BA08	0.59	13.53
CB08	0.55	17.11
CY08	0.46	16.75
ASK14	0.55	16.08
BSSA14	0.8	13.39
CB14	0.71	11.03
CY14	0.56	14.61

Although GMPEs provide spectral acceleration predictions across multiple periods, their most reliable and discriminative predictions typically occur at very short periods, where model-to-model variability is smallest and empirical constraints are strongest. For this reason, many regional GMPE screening studies rely on PGA or other short-period intensity measures as the primary basis for model selection (e.g., Boore et al., 2014; Chiou & Youngs, 2014; Kalkan & Gülkan, 2004; Karaca et al., 2021; Huang et al., 2023). Consistent with this practice, the current study evaluates GMPE performance using PGA—which is directly recorded, least affected by processing assumptions, and strongly correlated with Sa(T) at short periods ($T \leq 0.2$ s). In subsequent analyses (Section 4), GMPEs are not used to generate full response spectra; instead, they provide the short-period amplitude anchor on rock, while the long-period spectral characteristics are controlled by near-fault directivity effects and site-specific nonlinear amplification validated using the 2020 Samos earthquake. Thus, the use of PGA for GMPE screening is methodologically consistent with the intended application of the GMPEs in Section 4.

To better understand model-specific behavior, residual analyses were conducted for CB14 and BSSA14. Although both models performed well in terms of overall fit, they exhibited distinct systematic biases. CB14 tended to underpredict observed PGA, especially for short-distance and high-magnitude events. This behavior may be attributed to near-fault effects and local site amplification not fully accounted for in the model's global calibration. In contrast, BSSA14 showed a tendency to overpredict ground motions, particularly for low-magnitude and far-field events, suggesting that the model is conservative under low-shaking conditions. These trends are clearly illustrated in the residual plots in Figure 4a and 4b, where CB14 residuals are color-coded by magnitude.

These contrasting residual patterns underscore the limitations of applying globally calibrated GMPEs to complex local conditions without adjustment. Rather than indicating model inadequacy, they highlight the necessity for regionally validated ground motion models—especially in geologically heterogeneous urban basins like Izmir. These findings support a growing consensus in the literature advocating for localized GMPE calibration as a critical step toward improved seismic hazard assessment.

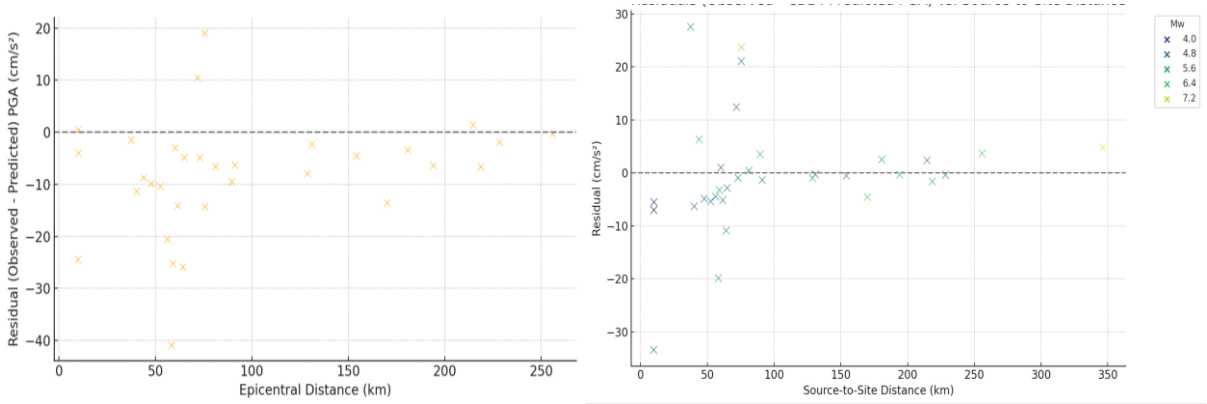

Figure 4. Residual plots for the two top-performing GMPEs: (a) BSSA14 – residuals vs distance (b) CB14 – residuals vs distance with magnitude color-coding.

3. Site response validation analysis for future predicted events

To simulate the site-specific seismic response for potential future scenarios, a validated one-dimensional (1D) Site Response Analysis (SRA) framework was adopted. The validation was performed using strong-motion recordings from the well-documented 2020 Samos (Sisam) Earthquake, which provided a rare and valuable opportunity to calibrate the numerical models under actual seismic loading conditions.

The earthquake occurred on October 30, 2020, with a moment magnitude of Mw 6.9, and an epicenter located approximately 14 km northeast of Samos Island in the Aegean Sea. Although the rupture occurred offshore, the event produced significant structural damage in Izmir due to its shallow focal depth, rupture directivity effects, and strong site amplification within the alluvial basin. Numerous strong-motion stations across Izmir recorded the event (Figure 5), including stations situated on soft alluvial soils and others positioned on rock outcrops. This diversity enabled a robust comparative evaluation of site effects (Kwok et al., 2007; Kramer, 1996).

The 1D SRA simulations were conducted by propagating the 3514 rock-outcrop motion—obtained from the AFAD strong-motion network—through the calibrated soil columns at the selected sites. Station 3514, characterized by a V_{S30} value of 836 m/s, is the only rock site in the study area and therefore provides an appropriate outcrop reference motion for validation purposes.

Four representative locations were selected to capture the geotechnical and geological variability across Izmir:

- Karşıyaka (3519) – basin edge, thick alluvial deposits
- Bayraklı (3513) – deep soft soils with high amplification potential
- Bornova (3522) – moderately deep alluvial layers
- Konak (central district) – urban area with transitional soil conditions

These stations collectively reflect the diversity of soil conditions and shaking characteristics across Izmir, enabling the development of a calibrated and reliable SRA model for subsequent scenario-based simulations.

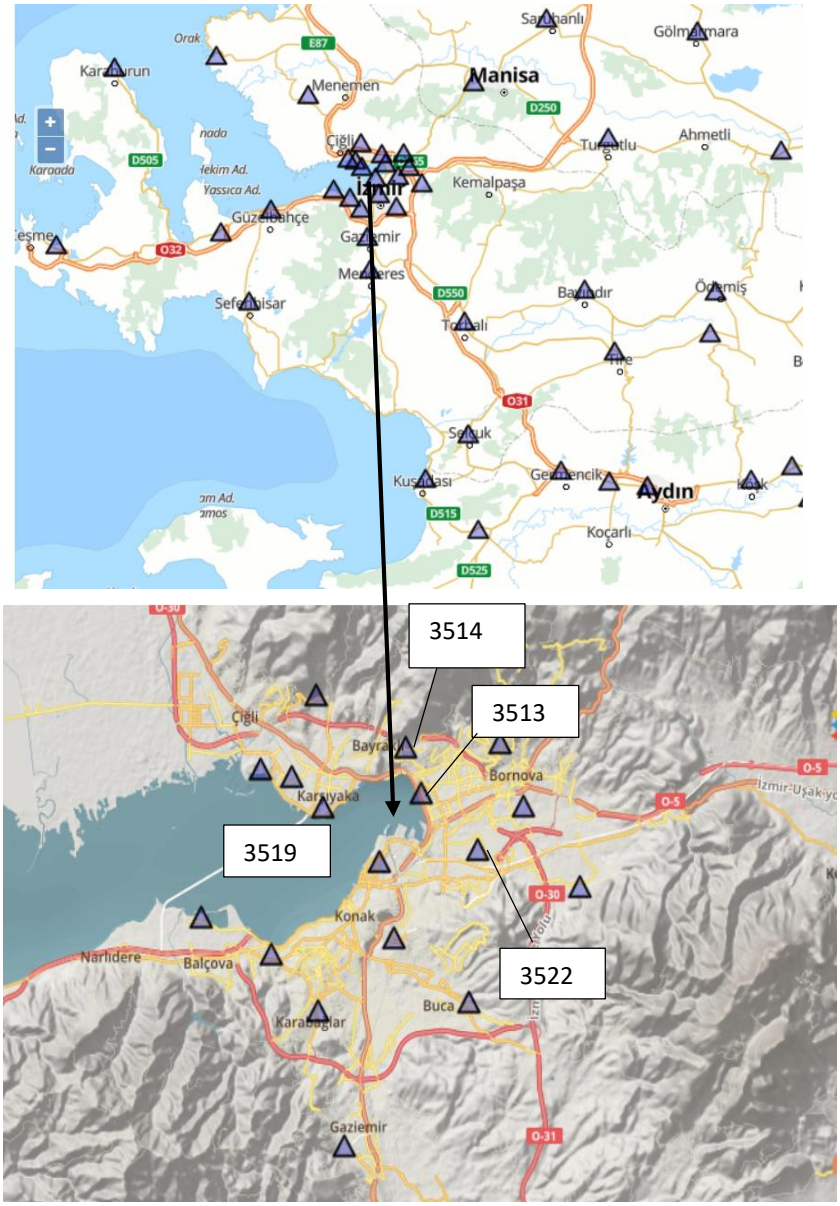

Figure 5. Overview of Stations in Izmir. (Base map adapted from AFAD TADAS (https://tadas.afad.gov.tr).)

The reference rock station was identified as Station 3514, located near the basin edge, and classified as a rock site based on its Vs_{30} = 836 m/s. The corresponding PGA values and geotechnical characteristics of all selected stations are presented in Table 4, while their geophysical profiles are illustrated in Figure 6.

By comparing observed ground motions with the site response simulations, the model's ability to reproduce frequency-dependent amplification patterns was evaluated. This validation step was critical to ensuring that the calibrated SRA models could be confidently applied to the simulation of future earthquake scenarios, particularly in geologically complex and amplification-prone zones of Izmir.

Table.4 Selected Soil/Rock Sites

Site Name	Region	Vs30 (m/sec)	TEC Site Class	Coordinates	PGA (g)
3514	Bayrakli	836.00	ZB	38.4762 27.1581	0.057 (N-S)
3513	Bayrakli	195.00	ZD	38.4584 27.1671	0.108 (N-S)
3519	Karsiyaka	131.00	ZE	38.4525 27.1112	0.153 (N-S)
3522	Bornova	249.00	ZD	38.4357 27.1987	0.075(N-S)

3.1. Soil Characterization and Nonlinear Site Response Modeling

Based on borehole logs, standard penetration test (SPT) profiles, and laboratory-based soil classification data, the upper 20 m of all three soil stations (3513, 3519, and 3522) predominantly consist of soft to medium-stiff fine-grained soils. These strata are interbedded and transitional in nature, comprising alternating sequences of low-plasticity clays (CL), high-plasticity clays (CH), and silty sands (SM). With increasing depth, the subsurface transitions into sandy clays (SC) and dense silty layers, which are characteristic of alluvial depositional environments. The soil profiles used in the analyses were compiled from deep geotechnical and geophysical investigations conducted at each station.

One-dimensional (1D) site response analyses were conducted using the DeepSoil software (Hashash et al., 2020), which allows for simulation of nonlinear soil behavior under vertically propagating shear waves. DeepSoil enables the incorporation of site-specific parameters, nonlinear modulus reduction and damping relationships, and realistic boundary conditions. The software has been widely applied in recent nonlinear site response studies (e.g., Cetin et al., 2022), and its reliability is further supported by experimental studies emphasizing the importance of modeling strain-dependent behavior (Tsai & Liu, 2017; Tsai & Li, 2024).

Modulus reduction (G/G_{max}) and damping ratio (D) curves were assigned based on soil classification. The Seed and Idriss (1970) model was used for cohesionless soils, while the Vucetic and Dobry (1991) curves were adopted for cohesive soils. The importance of accurate damping formulation was also emphasized by Zalachoris and Rathje (2015), who demonstrated through borehole array studies that nonlinear behavior and frequency-dependent damping are critical for reliable site response predictions across different strain levels.

Figure 6 presents SPT-N and shear-wave velocity (Vs) profiles for all soil sites and for the reference rock site (3514). The soil sites reflect soft alluvial conditions, whereas Station 3514—characterized by a Vs30 of 836 m/s and classified as NEHRP Site Class B—served as the reference rock motion for all SRA simulations. To accurately represent the deep basin geometry and ensure correct application of the input motion at the engineering bedrock level, each soil column was extended to its full geophysical depth. Based on regional MASW, microtremor, and

deep-borehole investigations, the total sediment thicknesses were defined as approximately 120 m for Station 3513, 250 m for Station 3519, and 90 m for Station 3522

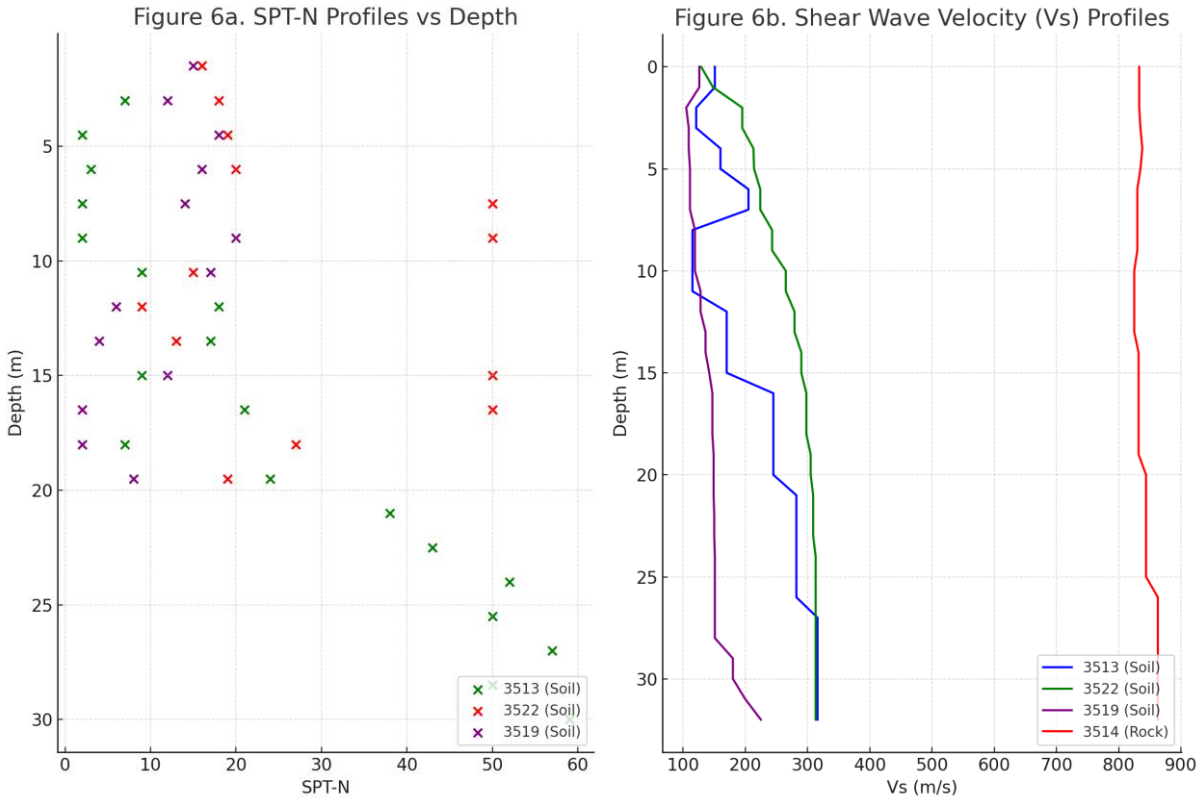

Figure 6. (a) SPT-N profiles vs. depth and (b) shear wave velocity (Vs) profiles for soil stations (3513, 3519, 3522) and reference rock station (3514).

3.2. Validation Results Using the 2020 Samos Earthquake

Site response analysis results were evaluated for three key locations across Izmir—Karşıyaka (3519), Bayraklı–Bornova (3522), and Konak–Alsancak (3513)—representing varying soil and geophysical conditions within the alluvial basin. The selection of multiple sites enabled assessment of spatial variability and the derivation of a generalized response spectrum that better reflects urban-scale ground motion behavior. Validation was conducted using the 2020 Samos Earthquake recordings, and the comparisons are illustrated in Figures 7 through 9.

In each case, spectral response functions derived from SRA were compared with observed site motions. The amplification function S_amp= SR (site) / SR (outcrop) was computed to evaluate frequency-dependent amplification. The station at Konak (3513) showed the most pronounced amplification, with peaks reaching 4.0–4.5 times the input motion at periods around 1.5 seconds. The Bornova station (3522) exhibited similar amplification characteristics, with peak values around 3.0–3.5 in the same period range. These stations share similar geotechnical conditions and are located within the central alluvial basin, which likely contributed to the consistent amplification behavior. In contrast, Karşıyaka station (3519) displayed notable amplification at longer periods, peaking near 2.5 seconds, suggesting differences in basin edge geometry and deeper soil layering effects.

These results illustrate the spatial heterogeneity of seismic site response within Izmir and highlight the limitations of using uniform design spectra across geologically diverse urban areas.

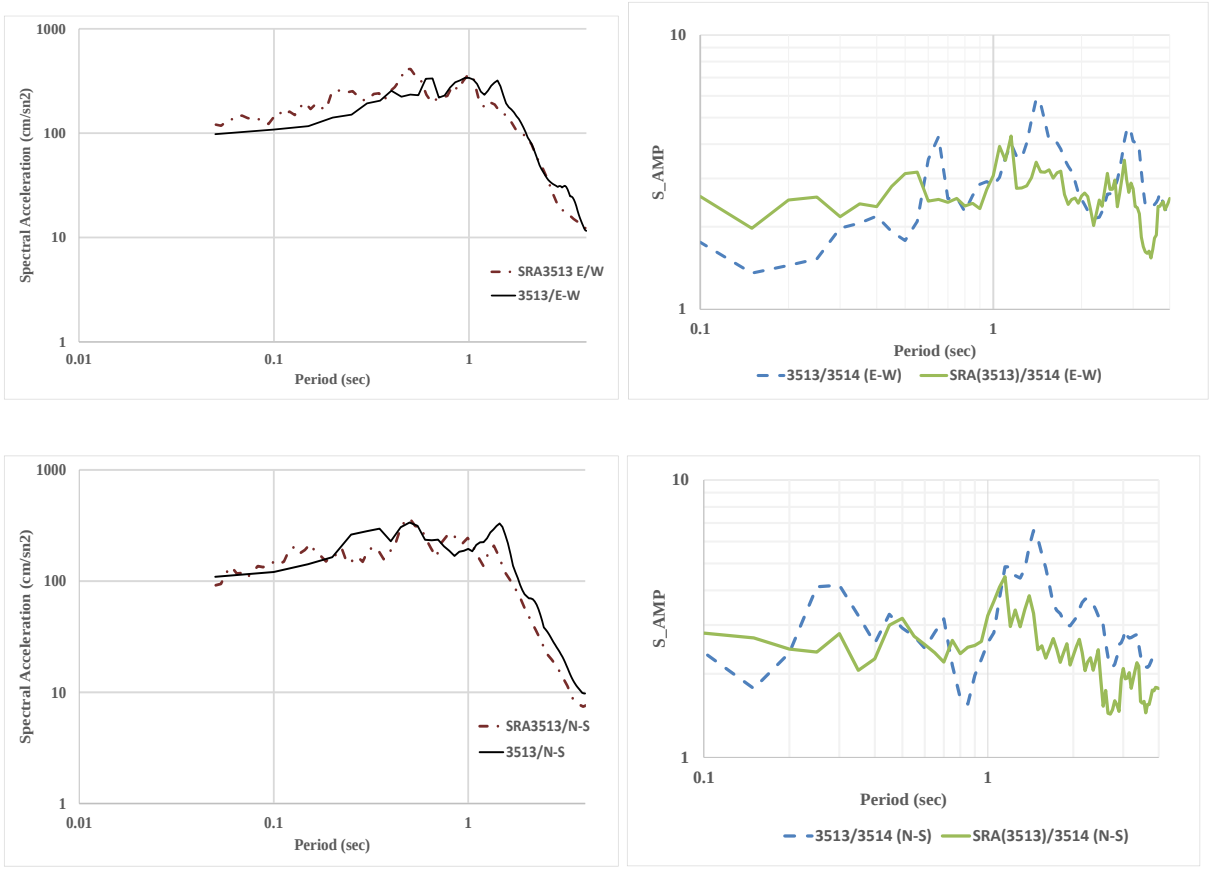

Figure 7. The comparison of recorded and estimated (SRA) elastic response and amplification spectra for 2020 Samos event@station 3513

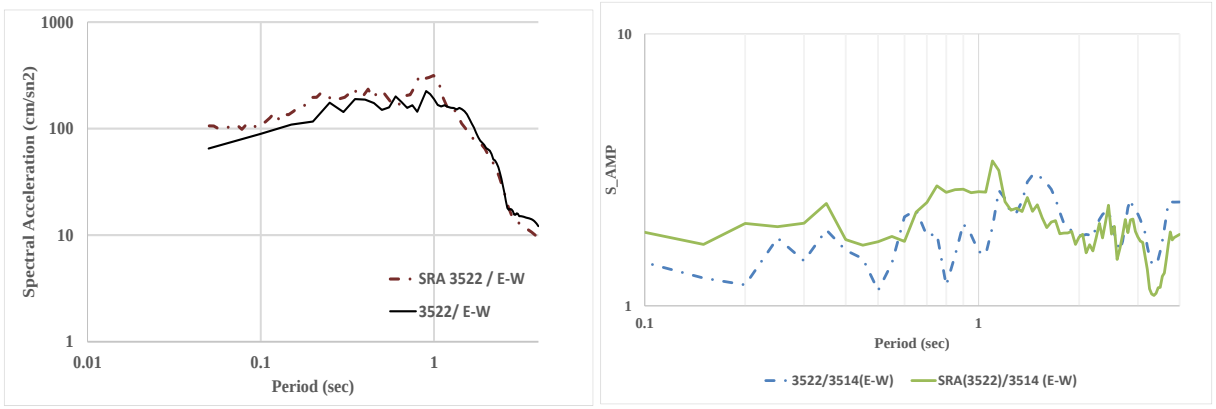

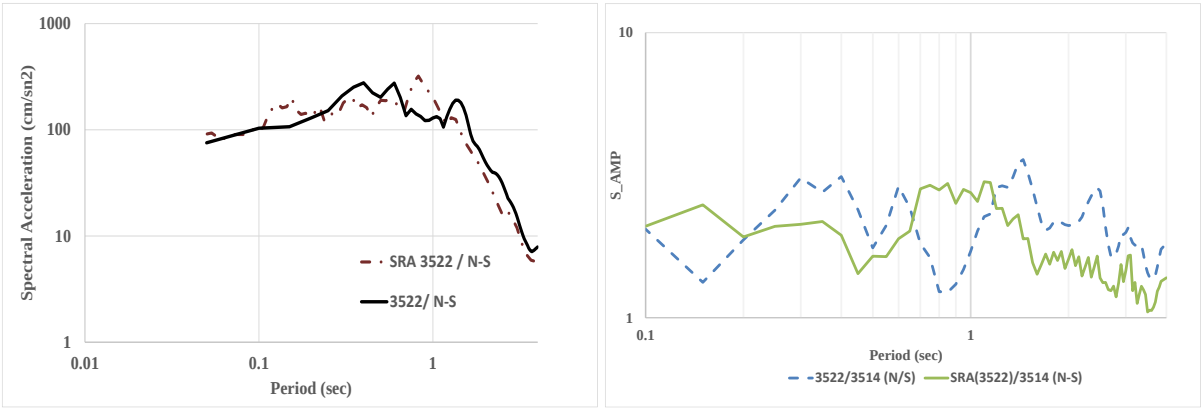

312

313 Figure 8. The comparison of recorded and estimated (SRA) elastic response and amplification spectra for 2020
314 Samos event@station 3522

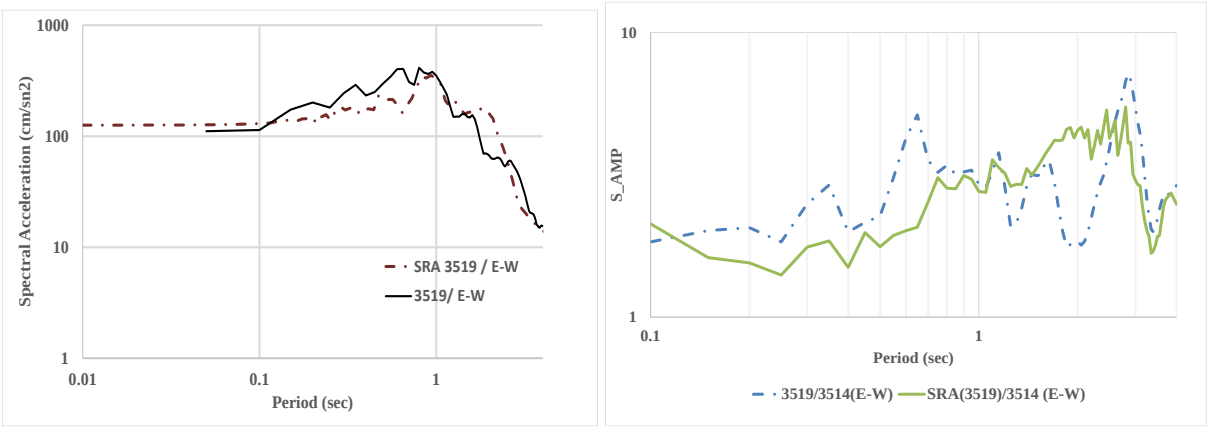

315

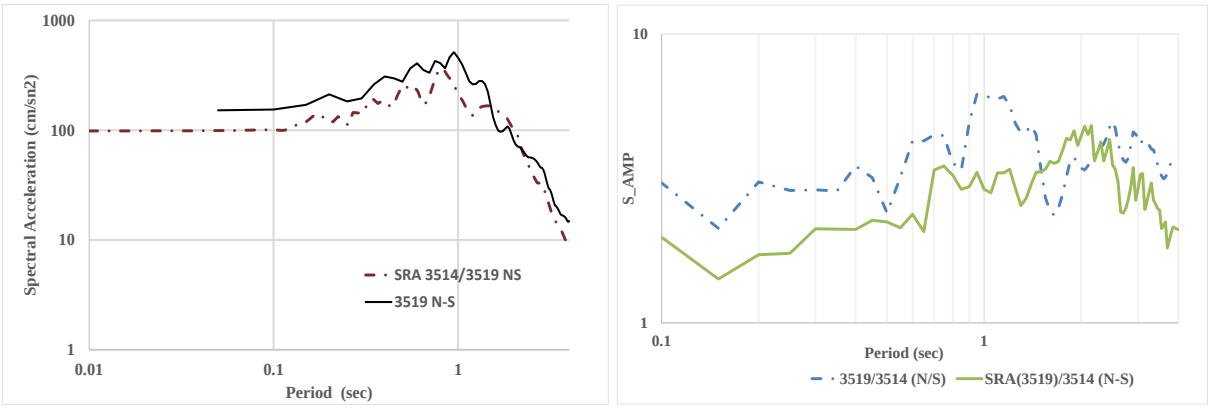

316

317 Figure 9. The comparison of recorded and estimated (SRA) elastic response and amplification spectra for 2020
318 Samos event@station 3519

319 The comparison between recorded and simulated acceleration response spectra demonstrates a strong agreement,
320 particularly within the period range of 0.5–1.5 seconds. This interval corresponds to the fundamental periods of
321 typical 6- to 10-story reinforced concrete (RC) buildings, which constitute a substantial portion of Izmir's existing

building stock. Therefore, amplification in this period range is of particular concern, as it directly increases seismic demand on mid-rise structures.

To quantitatively assess the accuracy of the site response simulations, the computed acceleration response spectra were compared with the corresponding recorded ground motion data at six different components (3513e-w, 3513n-s, 3522e-w, 3522n-s, 3519e-w, and 3519n-s). In addition to visual comparisons (see Figure 9), four quantitative metrics were employed to evaluate the degree of agreement between simulated and recorded spectra:

- Root Mean Square Error (RMSE) – measuring the average deviation,
- Coefficient of Determination (R^2) – indicating the proportion of variance explained,
- Goodness-of-Fit Index (GOF) – assessing relative error,
- Nash–Sutcliffe Efficiency (NSE) – evaluating predictive performance.

The computed values for each component are summarized in Table 5.

Table 5. Validation metrics between recorded and simulated acceleration response spectra.

Component	RMSE (cm/s²)	R^2	GOF	NSE
3513 E-W	49.36	0.797	0.881	0.797
3513 N-S	51.52	0.759	0.841	0.759
3522 E-W	53.82	0.481	0.831	0.481
3522 N-S	47.64	0.594	0.819	0.594
3519 E-W	60.5	0.73	0.841	0.73

As shown in Table 5, RMSE values ranged from 47.6 to 60.5 cm/s², reflecting moderate absolute deviations across components. R^2 values exceeded 0.73 in most cases, except for 3522 E–W, which exhibited lower correlation (R^2 = 0.481), likely due to localized variability in soil conditions or measurement noise. The GOF index remained consistently high (>0.81), and NSE values confirmed strong predictive agreement for most components.

In particular, the 3513 E–W and 3519 E–W components yielded the best fit, with $R^2 > 0.73$, GOF > 0.84, and NSE values supporting excellent agreement. These findings confirm the robustness of the nonlinear SRA model in capturing both the amplitude and spectral shape of the recorded ground motions, especially in soft soil zones with known amplification potential. On average, the 75th percentile of the observed spectra falls within the simulated spectral range, indicating reliable envelope matching across the mid-period band. Similar validation patterns were also reported by Cetin et al. (2024), supporting the consistency of the modeling framework employed in this study.

Based on these results, the adopted 1D site response framework is considered both reliable and transferable for future ground motion simulations. Combined with previously validated GMPE selection, this analysis provides a sound basis for generating site-specific target spectra and evaluating regional seismic demand scenarios. The next step involves defining target design spectra for scenario earthquakes and conducting corresponding SRA simulations across selected locations.

4. Selecting Target Response Spectrum And Evaluating The Results Of Future Events

In developing the target response spectrum for the deterministic Mw 6.5 scenario, the median predictions of the selected GMPEs (CB14 and BSSA14) were used primarily to anchor the short-period spectral amplitudes at the reference rock level. This is a common practice in regional seismic hazard studies, where PGA and very short-period Sa values provide a stable and well-constrained baseline. The longer-period portion of the spectrum, however, was shaped by additional physical considerations—including rupture directivity, basin effects, and the nonlinear site response characteristics validated in Section 3—rather than being taken directly from GMPE spectral shapes. This hybrid approach allows the target spectrum to remain consistent with both regional tectonic constraints and locally observed amplification patterns. Based on this framework, ground-motion parameters for the Mw 6.5 event were estimated in alignment with the RADIUS (1997) source definition for the Izmir Fault, whose magnitude potential is further supported by recent models such as EFSM20 and ESHM20.

Although the RADIUS model predates more recent fault datasets, its validity is corroborated by contemporary source characterizations such as EFSM20 (Basili et al., 2024), which classifies the Izmir Fault among the active structures with an estimated moment magnitude potential of Mw 6.5–6.7. Additionally, recurrence rate maps from ESHM20 (Danciu et al., 2024) indicate that the Izmir Basin exhibits annual exceedance rates on the order of $\log_{10} \approx -6.5$ to -7.0 for events exceeding Mw 6.5. These combined findings support the plausibility and engineering relevance of the selected scenario.

A critical factor in site-specific seismic hazard assessment is the near-fault rupture directivity effect, which can significantly amplify long-period ground motions. As originally proposed by Somerville et al. (1997), directivity-induced ground motions occur when seismic energy is focused along the rupture propagation direction, resulting in pulse-like waveforms with high amplitude and short duration. Such effects are particularly significant at sites located within approximately 10–15 km of the rupture plane.

Component-dependent spectral behavior was observed during the 2020 Samos Earthquake, particularly at Station 3519 (Mavişehir–Karşıyaka). A spectral comparison between horizontal components showed that the N–S component recorded spectral accelerations approximately 1.6 to 2.1 times greater than the transverse (E–W) component within the 1.0–2.0 second period range. Although this difference is most pronounced at Station 3519, similar directional tendencies with higher amplitudes in the N–S direction are also observed at the other stations examined in Section 3, albeit with smaller magnitude. Comparable directional amplification patterns have been reported in previous studies (Shahi and Baker, 2011; Chang et al., 2018; Bayless et al., 2024) in the long-period spectral range.

In light of these observations, directional characteristics of long-period ground motions were considered together with other relevant physical factors in the development of the target response spectrum. The selected spectrum was constructed to envelope the median predictions from the best-fitting GMPEs as well as the regulatory baseline defined by the Turkish Earthquake Code (TEC-2018). Special emphasis was placed on the 1.0–2.0 second period range, which is particularly relevant for mid- and high-rise structural response. The final deterministic design spectrum (Figure 10) thus integrates:

- regional seismic source characteristics,
- site-specific nonlinear amplification behavior,
- and empirical observations from near-fault recordings.

This spectrum serves as a robust basis for the performance-based evaluation of future seismic demand across Izmir's urban basin and provides a realistic representation of shaking intensity under near-fault ground motion conditions.

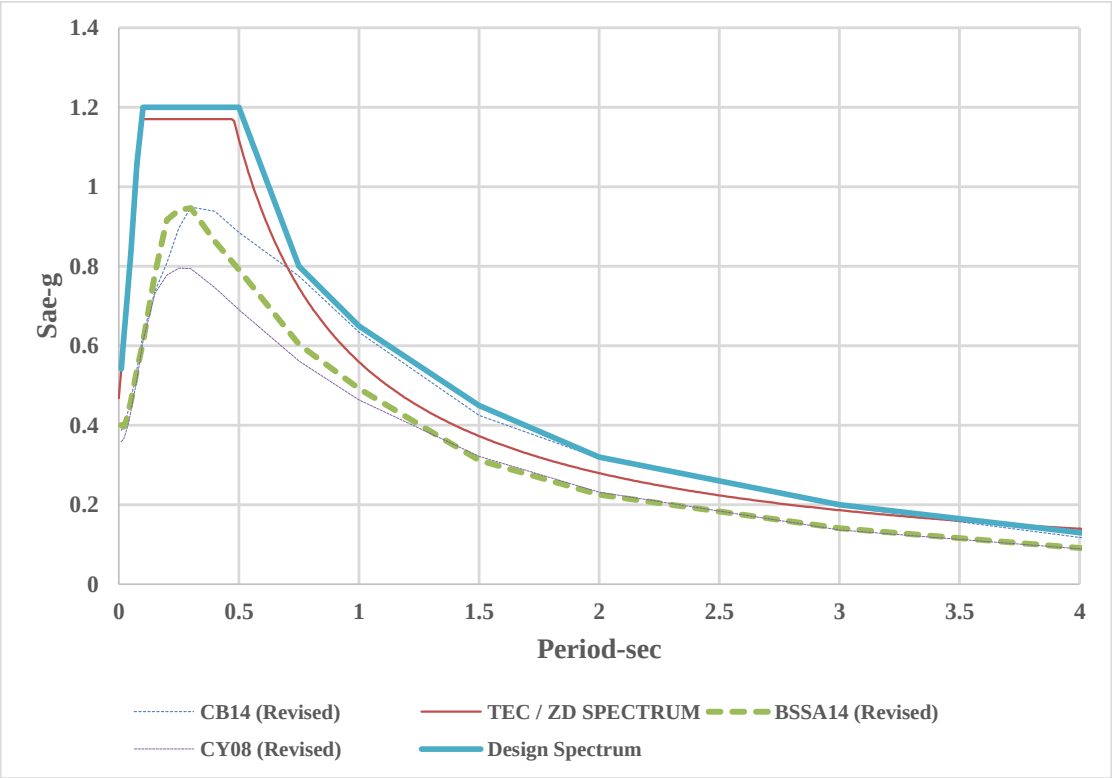

Figure 10. Proposed target response spectrum for the deterministic Mw 6.5 scenario, incorporating GMPE predictions, TEC-2018 provisions, and directivity-adjusted long-period amplification.

4.1. Ground Motion Selection and Spectral Matching

A total of 11 ground motion records were selected for the deterministic Mw 6.5 scenario (Table 6) and spectrally matched to the target response spectrum using SeismoMatch (Seismosoft, 2022). All ground-motion records listed in Table 6 were obtained from the PEER NGA-West2 Ground Motion Database. The matching was performed within the 0.1–2.0 s period range, which corresponds to the dominant periods of mid- to high-rise buildings in Izmir. The spectral matching algorithm preserved the nonstationary features and energy content of the original time histories while modifying their frequency content to achieve compatibility with the design spectrum.

405 Table 6. Selected Ground Motion Records

No	Record Sequence Number	Scale Factor	Earthquake Name	Year	Station Name	Magnitude	Mechanism	R_jb(km)	R_rup (km)	Vs30 (m/sec)
1	4881	2.32	Chuetsu-oki_Japan	2007	Nagaoka Kouiti Town	6.8	Reverse	11.61	20.77	294.38
2	549	1.91	Chalfant Valley-02	1986	Bishop-LADWP south St.	6.19	Strike Slip	14.38	17.17	303.47
3	6893	1.07	Darfield_New Zealand	2010	DFHS	7	Strike Slip	11.86	11.86	344.02
4	8133	4.31	Christchurch_New Zealand	2011	SLRC	6.2	Reverse Oblique	31.81	31.81	249.28
5	6971	2.12	Darfield_New Zealand	2010	SPFS	7	Strike Slip	29.86	29.86	389.54
6	882	2.57	Landers	1992	Desert Hot Springs	7.28	Strike Slip	26.84	26.84	344.67
7	4866	1.26	Chuetsu-oki_Japan	2007	Kawanishi Izumozaki	6.8	Reverse	0	11.75	338.32
8	4894	0.38	Chuetsu-oki_Japan	2007	Kashiwazaki NPP_Unit 1	6.8	Reverse	0	10.97	329
9	787	1.43	Loma Prieta	1989	Palo Alto - SLAC Lab	6.93	Reverse Oblique	30.62	30.86	425.3
10	1100	2.03	Kobe_Japan	1995	Abeno	6.9	Strike Slip	24.85	24.85	256
11	3979	2.82	San Simeon_CA	2003	Cambria-Hyw 1 Caltrans Bridge	6.52	Reverse	6.97	7.25	362.42

406

407 Note: The ground-motion records listed in Table 6 were accessed through the PEER NGA-West2 Ground Motion
408 Database. The original recordings were obtained from national and international strong-motion observation
409 networks, including the K-NET and KiK-net networks operated by the National Research Institute for Earth
410 Science and Disaster Resilience (NIED, Japan); strong-motion networks operated by the United States Geological
411 Survey (USGS) and the California Geological Survey (CGS), USA; and GeoNet, operated by GNS Science, New
412 Zealand

413 As illustrated in Figure 11, the matched spectra closely align with the target response spectrum. The mean spectrum
414 of the selected records remains within ±10% of the target over the defined period range, while the ±1σ envelope
415 effectively captures the record-to-record variability. This level of conformity satisfies compatibility guidelines
416 recommended by Eurocode 8 and PEER-GMSM protocols, which require the mean response spectrum to remain
417 within ±10% of the target and encourage representation of variability through mean ±1σ spectral envelopes (CEN,
418 2004; Haselton et al., 2011).

419

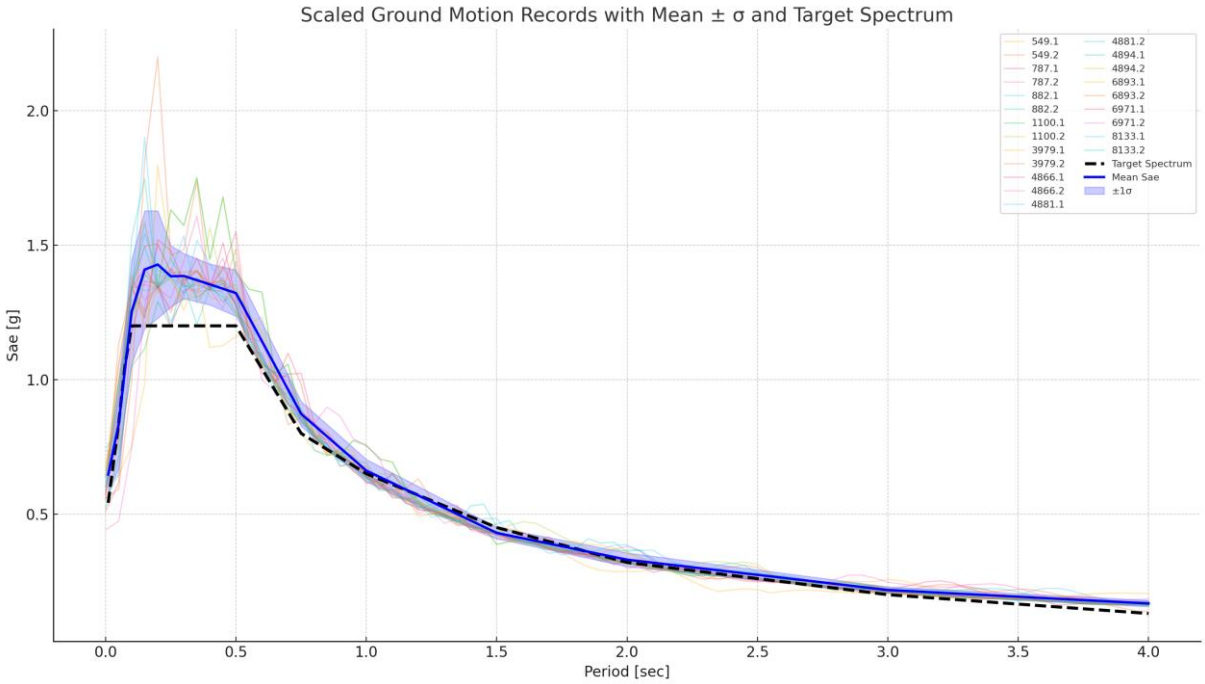

Figure 11. Combined plot showing scaled ground motion records, target spectrum (dashed), and the mean ±1σ spectral envelope of the records.

To further quantify the match quality, statistical metrics were computed at discrete periods. These include the mean spectral acceleration (Sae), standard deviation (σ), and the exceedance rate, defined as the proportion of records exceeding the target spectrum at each period. The results are summarized in Table 7.

The exceedance rate exceeds 90% for periods $T \leq 0.3$ s, indicating strong coverage in the short-period range. At longer periods ($T > 1.0$ s), the rate decreases, reflecting both the spectral shape of the selected ground motions and limitations in the scaling process. Nevertheless, the overall spectral compatibility satisfies performance-based ground motion selection criteria.

Table 7. Statistical summary of spectral accelerations (Sae) at selected periods: mean, standard deviation, and exceedance metrics relative to the target spectrum.

T (sec)	Target Sae (g)	Mean Sae (g)	Std Dev (g)	Exceed Count	Exceedance Rate
0.01	0.54	0.65	0.07	20.00	0.91
0.02	0.62	0.69	0.09	16.00	0.73
0.03	0.69	0.74	0.11	16.00	0.73
0.05	0.84	0.83	0.17	11.00	0.50
0.08	1.06	1.04	0.16	16.00	0.73
0.10	1.20	1.25	0.19	17.00	0.77
0.15	1.20	1.41	0.22	20.00	0.91
0.20	1.20	1.43	0.20	22.00	1.00
0.25	1.20	1.38	0.11	20.00	0.91
0.30	1.20	1.39	0.08	22.00	1.00
0.40	1.20	1.35	0.08	21.00	0.95
0.50	1.20	1.32	0.09	21.00	0.95
0.75	0.80	0.87	0.05	21.00	0.95
1.00	0.65	0.66	0.04	9.00	0.41
1.50	0.45	0.43	0.02	4.00	0.18

2.00	0.32	0.33	0.03	13.00	0.59
3.00	0.20	0.22	0.01	22.00	1.00
4.00	0.13	0.17	0.01	22.00	1.00

As shown in Figure 12, the exceedance rate distribution confirms strong representation in the short-period range and reasonable coverage at longer periods, supporting the robustness of the selected ground motion suite for site-specific nonlinear response analysis.

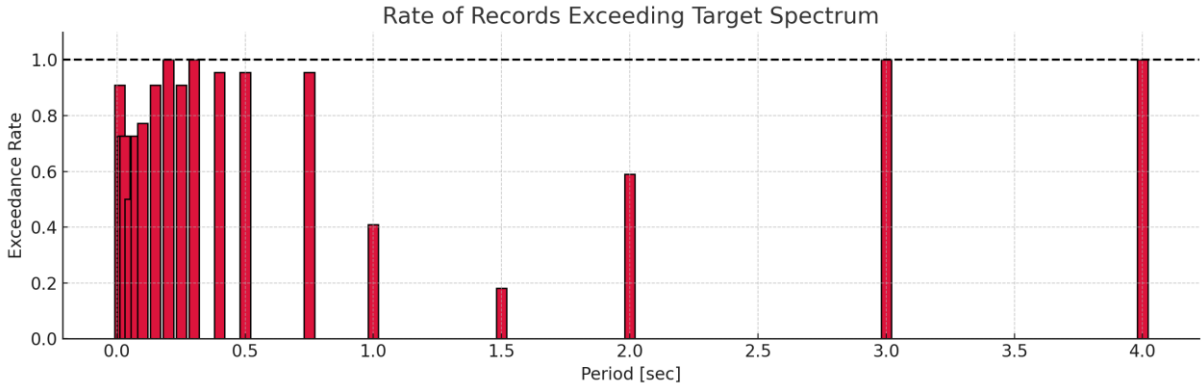

Figure 12. Rate of Records Exceeding Target Spectrum

In summary, the selected set of spectrally matched ground motions satisfies both code-based compatibility requirements and statistical representativeness. The resulting record suite provides a robust basis for deterministic nonlinear site response analysis, accurately capturing spectral variability across the period range of interest and supporting reliable performance-based seismic design and assessment.

4.2. Site-Specific Nonlinear Response Analysis and Comparison with Code-Based Spectra

Using the 1D nonlinear site response models calibrated in the previous sections via DEEPSOIL, site-specific ground response analyses were conducted for each station (3513 – Bayraklı, 3519 – Karşıyaka, and 3522 – Bornova) under the input of spectrally matched ground motion records. The spectral acceleration outputs at the surface are presented in Figure 13a-c, including the ensemble of scaled records, the mean ±1σ variability band, and the median response spectrum for each site.

The results indicate substantial variation in spectral amplification characteristics across stations, driven by differences in soil stiffness, stratigraphy, and nonlinear soil behavior. The ±1σ band serves as an envelope of epistemic uncertainty in record selection, while the median spectrum is used in subsequent engineering demand parameter (EDP) evaluations as a statistically robust representation of site-specific seismic input, in line with recommendations from PEER-GMSM Guidelines (Haselton et al., 2011).

In Bayraklı and Karşıyaka, which are underlain by deep alluvial deposits, spectral peaks shift toward longer periods ($T > 1.0$ s), suggesting basin-induced resonance effects (Borcherdt, 1994; Kaklamanos et al., 2013). In contrast, Bornova exhibits pronounced short-period amplification ($T < 0.5$ s) due to shallower, more compliant layers overlying stiff substrata.

Nonlinear behavior is especially evident in Karşıyaka, where broadened ±1σ dispersion and flattened median spectra suggest strain-softening, modulus degradation, and hysteretic damping, consistent with behavior described by Hashash et al. (2010) and Vucetic & Dobry (1991).

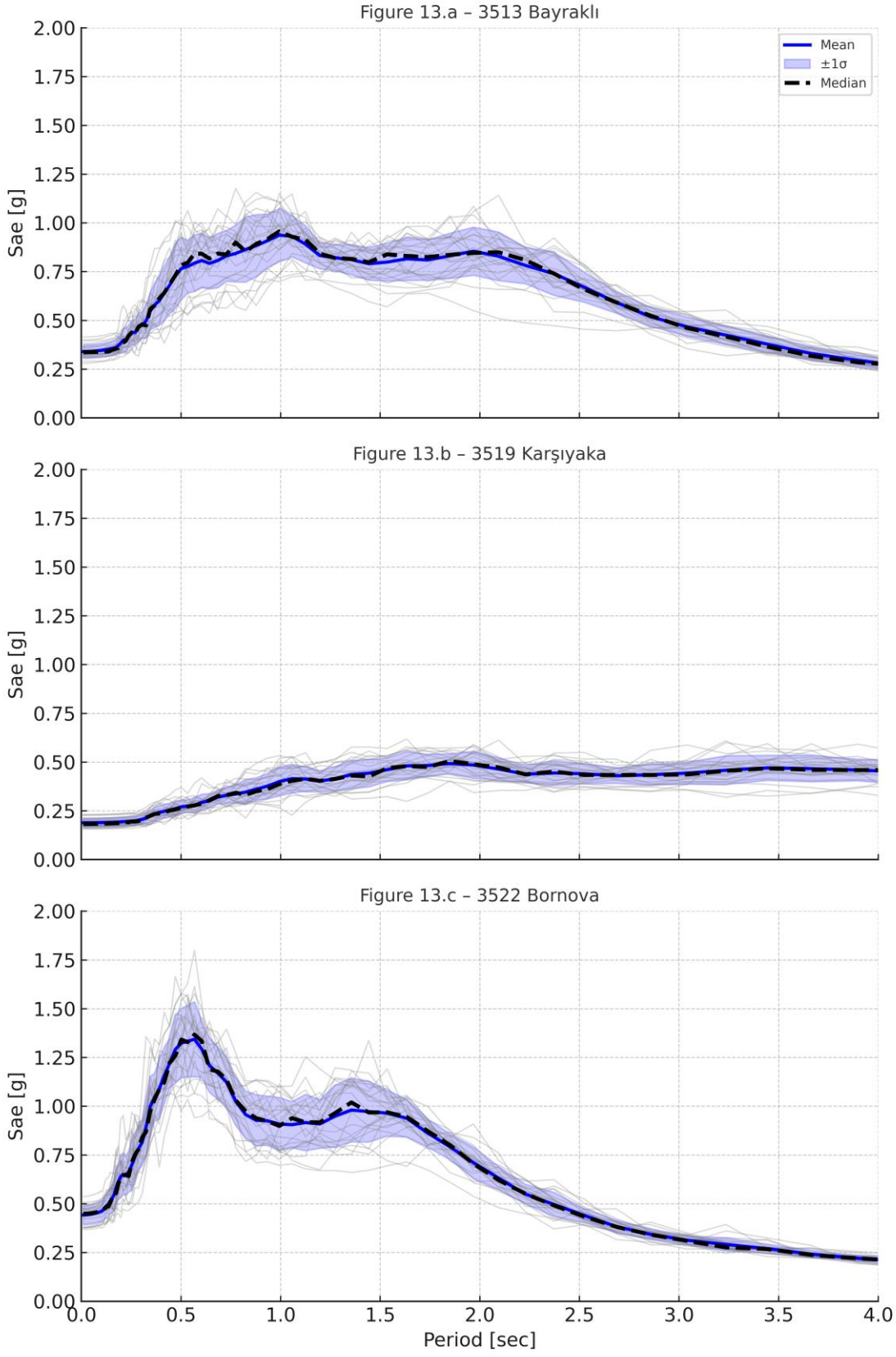

Figure 13. Scaled spectral acceleration (Sae) records for three selected sites: 3513 – Bayraklı, (**b**) 3519 – Karşıyaka, and (**c**) 3522 – Bornova. Each subplot includes the ensemble of scaled motions (gray lines), the mean spectrum (blue), ±1σ variability band (shaded), and the median response spectrum (black dashed)

Figure 14 compares the median spectra from SRA with the uniform hazard spectrum (UHS) and code-defined design spectra (TEC, 2018) for Site Classes ZE and ZD. Across all three sites, clear deviations are observed:

- Bayraklı and Karşıyaka: Peak amplifications occur in T > 1.0 s range—significantly exceeding TEC curves.
- Bornova: Amplification is dominant in T < 0.5 s range, revealing frequency-dependent site response.

These differences demonstrate that code-based spectral shapes do not adequately reflect site-specific effects in deep alluvial environments.

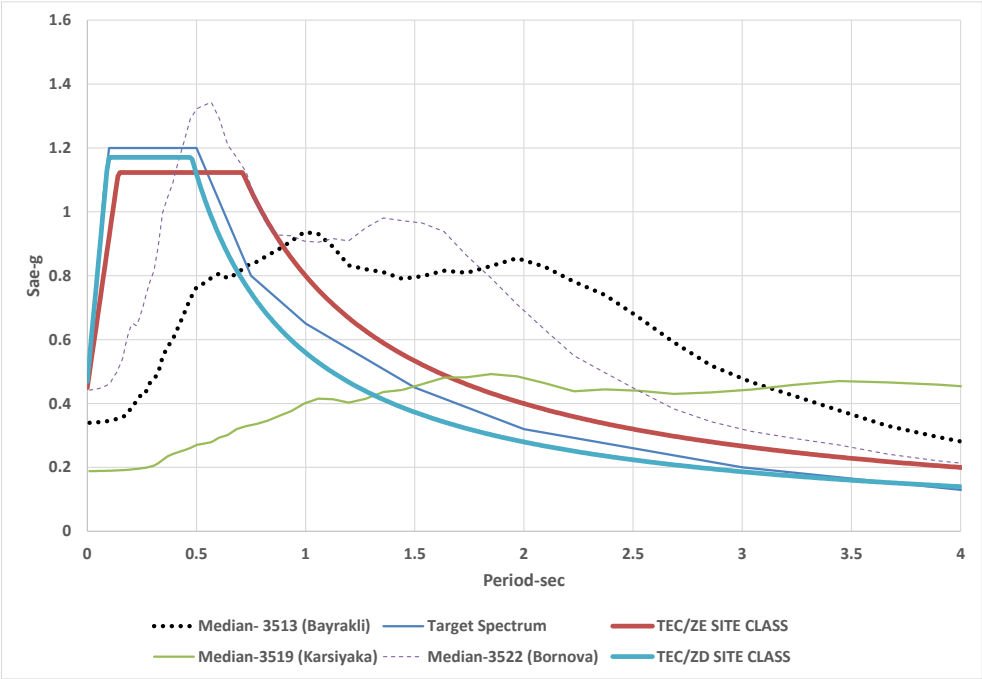

Figure 14. Median spectral acceleration (Sae) curves obtained from scaled ground motions for three different sites (Bayraklı, Karşıyaka, Bornova), compared with the uniform hazard spectrum (Target Spectrum) and the regulatory spectra defined in the Turkish Earthquake Code (2018) for Site Classes ZE and ZD.

According to TEC, the effect of local soil conditions is incorporated through two modification factors, FS and F1, which are used to calculate the design spectral acceleration values as follows:

$$S_{ds}=S_S \cdot F_S \text{ and } S_{d1}=S_1 \cdot F_1 \quad (2)$$

where:

- Sds is the design spectral acceleration for short-period structures (typically affecting low-rise buildings),

- Sd1 is the design spectral acceleration at a 1.0-second period (affecting mid- to high-rise buildings),
- S_S and S_1 are the reference spectral accelerations on rock or firm soil (Type A/B),
- F_S and F_1 are site amplification factors defined in TEC based on soil class (e.g., ZE, ZD).

However, results of the site-specific response analyses revealed that the actual site amplification ratios (SAR) derived from ground motion simulations significantly exceed the TEC-defined values, particularly for F1, which controls long-period demands. These findings are summarized in Table 8, where the ratio of F1_SAR to F1_TEC demonstrates the magnitude of underestimation in current code-based designs.

Table 8. Local site modification factors (F1) according to TEC and SAR of scenario earthquake

Station	Vs30	Soil Class (Acc TEC)	F1/ TEC	F1/ SAR, t=1 sec
3513	195	ZD	2.054	4.21
3522	249	ZD	2.054	4.76
3519	131	ZE	2.935	4.40

4.3. Engineering Implications for Performance-Based Design

This amplification behavior has critical design implications, particularly for reinforced concrete (RC) moment-resisting frames with 3 to 10 stories, which have fundamental periods in the 0.5–1.5 s range. According to TEC (2018), such structures are expected to meet:

- Life Safety (LS) under the Design Earthquake (DD-2)**,** and
- Collapse Prevention (CP) under the Maximum Considered Earthquake (DD-1)**.**

However, in sites like Bornova, the median spectral acceleration at T = 1.0 s exceeds the TEC value by a factor of 4.76. This discrepancy may result in:

- Underestimation of interstory drift demands,
- Increased likelihood of plastic hinge formation,
- Potential exceedance of performance limits, even when structures comply with code-based spectra.

Therefore, these findings underscore the necessity of refining design input parameters—either by modifying the amplification factor F_1 or adopting fully site-specific response spectra—to ensure accurate seismic demand estimation and adequate structural performance on deep soft soils.

This conclusion aligns with international research (e.g., Stewart & Seyhan, 2013; Pitilakis et al., 2013), which has shown that empirical site-class-based amplification factors often underestimate long-period spectral demands, particularly in sedimentary basins with complex stratigraphy and low shear-wave velocities.

5. Summary and Conclusions

5.1. Summary of the methodology

This study aimed to assess site-specific seismic demands for the city of Izmir by integrating empirical ground motion data, GMPE evaluation, and 1D nonlinear site response analyses. The major components of the methodology and key findings are summarized as follows:

- Firstly, using a dataset of past recorded earthquake events, the level of agreement with current GMPE equations was investigated. Based on the residual analysis, two GMPEs were selected that showed the best consistency with the observed recordings in Izmir, and were subsequently used for defining target spectrum parameters in the site-specific seismicity analysis. Despite being NGA-West2 models, these GMPEs exhibited systematic residuals reaching up to ±0.3 log units, indicating the necessity for regionally calibrated models for Izmir.
- To perform site-specific seismic analyses, well-recorded event of Izmir-Samos earthquake data were utilized. A 1D analysis model, using the available geotechnical data was applied for 3 different stations. These stations were selected for the aim to
    - represent different alluvial soil conditions of the city
    - take in to account of the 3 most populated, therefore representative regions of the city
    - be able to arrive a more general conclusion about the possible future earthquake simulations
- A future deterministic scenario earthquake with Mw = 6.5 was developed for the Izmir Fault, following the RADIUS (2005) framework and supported by recent tectonic models. The resulting target spectrum was enhanced by incorporating near-field and directivity effects, resulting in significant modifications to spectral shape and amplitude—particularly at intermediate and long periods. The modified target spectrum exhibits 65–80% higher amplitudes compared to the TEC (2018) code spectra for ZE and ZD classes over the T = 0.3–1.0 s range. To maintain regulatory consistency, the TEC (2018) was also used to define the baseline hazard level corresponding to a 475-year return period (i.e., 10% probability of exceedance in 50 years).
- Eleven recorded strong ground motions were selected and spectrally matched to the scenario-specific target spectrum using SeismoMatch. These matched records were used as input for 1D nonlinear simulations at the three selected sites, enabling deterministic estimation of surface-level spectral accelerations under future earthquake conditions.

5.2. Key Findings

The key findings of this study are as follows:

- **Validation with the 2020 Samos Earthquake:** The 2020 Samos earthquake has been a significant event for site-specific seismicity studies due to the abundance of recording stations and the rich data content available. Analyses based on this event showed distinct spectral amplifications, particularly in the long-period range (T > 1.0 s), which is critical for mid- and high-rise building design.
- **GMPE Evaluation and Region-Specific Spectral Characterization**: Residual-based comparisons of GMPEs enabled the selection of the most appropriate models for Izmir. Despite their global robustness,

the selected NGA-West2 models exhibited systematic residuals up to ±0.3 log units, emphasizing the need for regionally calibrated ground motion models that better reflect Izmir's unique tectonic and geotechnical conditions.

- **Effect of Directivity and Near-Fault Conditions on the Target Spectrum:** By incorporating rupture directivity and near-field effects, the target spectrum was significantly enhanced, particularly within the 0.5–1.5 s period range. Compared to the standard code-based spectra (TEC, 2018), the resulting spectrum showed 65–80% higher spectral accelerations, underscoring the importance of including these effects in future national code revisions.
- **Observed Site Amplification and Implications for Design Parameters**: Site-specific simulations revealed that surface spectral acceleration at T = 1.0 s was amplified by factors of 2.5 to 4.8, depending on location. The median response spectra yielded the following amplification ratios when compared to TEC-based F_1 values:
    - Bornova: Sa = 0.91 g vs. TEC = 0.19 g → F_1 ratio = 4.76
    - Bayraklı: Sa = 0.73 g vs. TEC = 0.19 g → F_1 ratio = 3.84
    - Karşıyaka: Sa = 0.56 g vs. TEC = 0.19 g → F_1 ratio = 2.93

These findings clearly indicate that the site amplification factors (F_1) in the Turkish Earthquake Code significantly underestimate long-period demand, particularly in deep alluvial basins.

- **Design Relevance for Critical Building Classes:** The underestimation is especially critical for 3–10 story reinforced concrete moment-resisting frame structures, whose natural periods (T = 0.5–1.5 s) fall within the affected range. These buildings are typically designed to meet Life Safety (LS) under the Design Earthquake (DD-2) and Collapse Prevention (CP) under the Maximum Considered Earthquake (DD-1) per TEC (2018). Failure to account for local amplification may lead to:
    - Underestimation of interstory drift,
    - Inadequate detailing for plastic hinge zones,
    - Potential exceedance of performance thresholds.
- **Representativeness of Site Selection and Implications for Basin-Wide Analysis:** The selection of three sites (Bayraklı, Karşıyaka, Bornova) provided a basis for understanding the variability of seismic response across Izmir. This approach lays the groundwork for future studies exploring basin effects, nonlinear soil behavior, and wave propagation phenomena in more complex 2D/3D models.
- **Need for Region-Specific Seismic Design Frameworks:** The residual trends observed in the GMPE evaluations—despite using globally recognized models—reinforce the need for site-specific and regionally adjusted ground motion models in seismic hazard mitigation. These findings support a growing consensus in the literature that generic site classification frameworks are insufficient in deep sedimentary basins with significant impedance contrasts and complex source mechanisms.

5.3. Limitations and Recommendations for Future Work

While the present study provides valuable insights into local site amplification and spectrum compatibility in Izmir, several limitations should be acknowledged to guide future research:

First, the site response analyses were conducted using 1D equivalent-linear models, calibrated with available geotechnical and seismic data. Although these models are widely accepted for practical applications, they do not fully capture three-dimensional basin effects, such as lateral wave propagation, edge-generated surface waves, and spatial variability in soil layering and shear-wave velocity. Incorporating 2D or 3D nonlinear models would improve the accuracy of response predictions, especially in complex alluvial basins like Izmir.

Second, the study adopted a deterministic Mw = 6.5 earthquake scenario, based on the Izmir Fault. While this provides valuable insight into scenario-based seismic demands, it limits the exploration of multi-source interactions and epistemic uncertainties inherent in probabilistic seismic hazard assessments (PSHA). Future work should integrate probabilistic frameworks to account for the full range of potential seismic sources, magnitudes, and recurrence rates.

Third, the spectrally matched ground motions were scaled to a single intensity level (e.g., 475-year return period). While this is consistent with design-level evaluation, it may not adequately address varying intensity measure levels (IMLs) required for performance-based seismic design (PBD) or fragility analysis. Future studies should incorporate multi-level hazard scenarios to capture demand variability and damage probability more comprehensively.

To address these limitations and advance the regional seismic assessment framework, future research could explore:

- Fully nonlinear time-domain simulations, accounting for strain-dependent soil behavior and cyclic degradation,
- 3D geotechnical modeling, especially for large-scale basin structures and lateral heterogeneity,
- Machine-learning-based surrogate modeling, to improve computational efficiency and enable real-time seismic risk screening across urban areas.

Although this study is rooted in the geotechnical and tectonic conditions of Izmir, the developed methodology offers a generalizable and transferable framework for other seismically active urban areas underlain by deep alluvial or sedimentary basins. By integrating residual-based GMPE selection, site-specific spectrum development, and nonlinear site response analysis, this study bridges the gap between code-level design assumptions and localized seismic demand.

Ultimately, the findings contribute to the development of a more resilient seismic design paradigm, emphasizing the critical role of site-specific response analysis in modern performance-based engineering, particularly for infrastructure located in complex geologies where empirical code factors may not suffice.

Funding The authors declare that no funds, grants, or other support were received during the preparation of his manuscript.

Data availability all data and models analyzed during the current study are available from the corresponding author on reasonable request.

Declarations

Competing interests the authors have no relevant financial or non-financial interests to disclosure.

Acknowledgements The authors gratefully acknowledge AFAD for providing the strong-motion recordings of the 2020 Samos Earthquake, and the Pacific Earthquake Engineering Research Center (PEER) for maintaining and providing access to the NGA-West2 ground-motion database. The continuous efforts of the contributing observation networks and institutions are sincerely appreciated

6. References

Abrahamson NA, Silva W. Summary of the Abrahamson & Silva NGA groundmotion relations. Earthq Spectra 2008;24:67–97. https://doi.org/10.1193/1.2924360

Abrahamson NA, Silva WJ, Kamai R. Summary of the ASK14 ground motion relation for active crustal regions. Earthq Spectra 2014;30:1025–55. https://doi.org/10.1193/070913EQS198M

Akyol, N., Zhu, L., Mitchell, B. J., Sözbilir, H., & Kekovalı, K. (2006). Crustal structure and local seismicity in western Anatolia. Geophysical Journal International, 166(3), 1259–1269. https://doi.org/10.1111/j.1365-246X.2006.03053.x

Akkar, S., & Bommer, J. J. (2010). Empirical equations for the prediction of PGA, PGV, and spectral accelerations in Europe, the Mediterranean region, and the Middle East. Seismological Research Letters, 81(2), 195–206. https://doi.org/10.1785/gssrl.81.2.195

Akkar, S., Sandıkkaya, M. A., & Bommer, J. J. (2014). Empirical ground-motion models for point- and extended-source crustal earthquake scenarios in Europe and the Middle East. Bulletin of Earthquake Engineering, 12(1), 359–387. https://doi.org/10.1007/s10518-013-9461-4

Basili, R., Danciu, L., Beauval, C., Sesetyan, K., Vilanova, S. P., Adamia, S., Arroucau, P., Atanackov, J., Baize, S., Canora, C., Caputo, R., Carafa, M. M. C., Cushing, E. M., Custódio, S., Demircioglu Tumsa, M. B., Duarte, J. C., Ganas, A., García-Mayordomo, J., Gómez De La Peña, L., … Giardini, D. (2024). The European Fault-Source Model 2020 (EFSM20): geologic input data for the European Seismic Hazard Model 2020. Natural Hazards and Earth System Sciences, 24(11). https://doi.org/10.5194/nhess-24-3945-2024

Bayless, J., Abrahamson, N. A., & Somerville, P. (2024). A rupture directivity adjustment model and its application in seismic hazard analysis. Earthquake Spectra.

Boore DM, Atkinson GM (2008) Ground-motion prediction equations for the average horizontal component of PGA, PGV, and 5%-damped PSA at spectral periods between 0.01 s and 10.0 s. Earthq Spectra 24:99–138. https://doi.org/10.1193/1.2830434

Boore DM, Stewart JP, Seyhan E, Atkinson GM. NGA-West2 equations for predicting PGA, PGV, and 5% damped PSA for shallow crustal earthquakes. Earthq Spectra 2014;30:1057–85. https://doi.org/10.1193/070113EQS184M

Borcherdt, R. D. (1994). Estimates of site-dependent response spectra for design (methodology and justification). Earthquake Spectra, 10(4), 617–653. https://doi.org/10.1193/1.1585791

Campbell KW, Bozorgnia Y. NGA ground motion model for the geometric mean horizontal component of PGA, PGV, PGD and 5% damped linear elastic response spectra for periods ranging from 0.01 to 10 s. Earthq Spectra 2008;24:139–71. https://doi.org/10.1193/1.2857546

Campbell KW, Bozorgnia Y. NGA-West2 ground motion model for the average horizontal components of PGA, PGV, and 5% damped linear acceleration response spectra. Earthq Spectra 2014;30:1087–115. https://doi.org/10.1193/062913EQS175M.

CEN. (2004). Eurocode 8: Design of structures for earthquake resistance – Part 1: General rules, seismic actions and rules for buildings (EN 1998-1:2004). Brussels: European Committee for Standardization.

Cetin, K. Ö., Altun, S., Askan, A., Akgün, M., Sezer, A., Kıncal, C., ... & Karaali, E. (2022). The site effects in Izmir Bay of October 30, 2020, M7.0 Samos Earthquake. Soil Dynamics and Earthquake Engineering, 152, 107051. https://doi.org/10.1016/j.soildyn.2021.107051

Cetin, K. Ö., Zarzour, M., Çakır, E., Tuna, S. Ç., & Altun, S. (2023). 2-D and 3-D basin site effects in Izmir–Bayrakli during the October 30, 2020 Mw7.0 Samos earthquake. Bulletin of Earthquake Engineering, 21, 5419–5442. https://doi.org/10.1007/s10518-023-01738-3

Cetin, K.O., Cakir, E. & Zarzour, M. Seismic site effect models for the Turkiye-Izmir-Bayrakli Basin. Bull Earthquake Eng 22, 303–328 (2024). https://doi.org/10.1007/s10518-023-01774-z

Chang, Z., Sun, X., Zhai, C., Zhao, J. X., & Xie, L. (2018). An empirical approach of accounting for the amplification effects induced by near fault directivity. Bulletin of Earthquake Engineering, 16(5), 1871–1885.

Chiou, B.S.J. and Youngs, R.R. (2008) An NGA Model for the Average Horizontal Component of Peak Ground Motion and Response Spectra. Earthquake Spectra, 24, 173-215. https://doi.org/10.1193/1.2894832

Chiou BSJ, Youngs RR. Update of the Chiou and Youngs NGA model for the average horizontal component of peak ground motion and response spectra. Earthq Spectra 2014;30:1117–53. https://doi.org/10.1193/072813EQS219M

Dan McKenzie, Active tectonics of the Alpine—Himalayan belt: the Aegean Sea and surrounding regions, Geophysical Journal International, Volume 55, Issue 1, October 1978, Pages 217–254, https://doi.org/10.1111/j.1365-246X.1978.tb04759.x

Danciu, L., Giardini, D., Weatherill, G., Basili, R., Nandan, S., Rovida, A., Beauval, C., Bard, P.-Y., Pagani, M., Reyes, C. G., Sesetyan, K., Vilanova, S., Cotton, F., and Wiemer, S.: The 2020 European Seismic Hazard Model: overview and results, Nat. Hazards Earth Syst. Sci., 24, 3049–3073, https://doi.org/10.5194/nhess-24-3049-2024, 2024.

Emre, Ö., Duman, T.Y., Özalp, S. et al. Active fault database of Turkey. Bull Earthquake Eng 16, 3229–3275 (2018). https://doi.org/10.1007/s10518-016-0041-2

Emre O, Ozalp S, Dogan A, Ozaksoy V, Yildirim C, Goktas F (2005) Active faults in the vicinity of Izmir and their earthquake potentials [in Turkish], Report No: 10754, Geological Studies Department, General Directorate of Mineral Research and Exploration, Ankara, Turkey

FEMA (2001). NEHRP recommended provisions for seismic regulations for new buildings and other structures (FEMA 368). Washington, DC: Federal Emergency Management Agency.

Gülerce, Z., Akbaş, B., Özacar, A. A., Sopacı, E., Önder, F. M., & Bora, S. S. (2022). Predictive performance of current ground motion models for recorded strong motions in 2020 Samos Earthquake. Soil Dynamics and Earthquake Engineering, 152, 107053. https://doi.org/10.1016/j.soildyn.2021.107053

Haselton, C. B., Baker, J. W., Liel, A. B., Deierlein, G. G., Bozorgnia, Y., & Curtin, P. (2011). Evaluation of ground motion selection and modification methods: Predicting median interstory drift response of buildings (PEER Report No. 2011/03). Pacific Earthquake Engineering Research Center, University of California, Berkeley.

Hashash, Y. M. A., Park, D., & Phillips, C. A. (2010). Evaluation of ground motion analysis procedures for seismic design of deep foundations. PEER Report 2010/05, University of California, Berkeley.

Hashash YMA, Musgrove MI, Harmon JA, Ilhan O, Xing G, Numanoglu O. DEEPSOIL V7.0, User manual. Urbana, IL: Board of Trustees of University of Illinois at Urbana-Champaign; 2020

Kaklamanos, J., Baise, L. G., Boore, D. M., & Thompson, E. M. (2013). Implementation of a VS30-based nonlinear site amplification model for NEHRP site classes C and D in the NGA-West2 database. Bulletin of the Seismological Society of America, 103(1), 211–228. https://doi.org/10.1785/0120120195

Kalkan, E., & Gülkan, P. (2004). Site-dependent spectra derived from ground-motion records Turkey. Earthquake Spectra, 20(4), 1111–1138. https://doi.org/10.1193/1.1810233

Kramer SL (1996) Geotechnical earthquake engineering, Prentice Hall, Upper Saddle River

Kwok, A. O. L., Stewart, J. P., Hashash, Y. M. A., Matasovic, N., Pyke, R., Wang, Z., & Yang, Z. (2007). Use of Exact Solutions of Wave Propagation Problems to Guide Implementation of Nonlinear Seismic Ground Response Analysis Procedures. Journal of Geotechnical and Geoenvironmental Engineering, 133(11). https://doi.org/10.1061/(asce)1090-0241(2007)133:11(1385)

Ocakoğlu, F., Demirbağ, E., & Kuşçu, İ. (2005). Neotectonic structures in Izmir Gulf and surrounding regions (western Turkey): Evidences of strike-slip faulting with compression in the Aegean extensional regime. Marine Geology, 219(2–3), 155–171. https://doi.org/10.1016/j.margeo.2005.06.004

Pitilakis, K., Riga, E., & Anastasiadis, A. (2013). New code site classification, amplification factors and normalized response spectra based on a worldwide ground-motion database. Bulletin of Earthquake Engineering, 11(4). https://doi.org/10.1007/s10518-013-9429-4

RADIUS (1997), Risk assessment tools for diagnosis of urban areas against seismic disaster Izmir earthquake master program, Bogazici University Kandilli Observatory, Istanbul, Turkey

Seed, H. B., and Idriss, I. M. (1970). "Soil moduli and damping factors for dynamic response analyses," Report No. EERC 70-10, Earthquake Engineering Research Center, Univ. of California, Berkeley, California.Berkeley, December.

Seismosoft. (2022). SeismoMatch v2022 – Spectrum matching software. https://seismosoft.com

Shahi, S. K., & Baker, J. W. (2011). An empirically calibrated framework for including the effects of near-fault directivity in probabilistic seismic hazard analysis. Bulletin of the Seismological Society of America, 101(2), 742–755.

Somerville, P. G., Smith, N. F., Graves, R. W., & Abrahamson, N. A. (1997). Modification of empirical strong ground motion attenuation relations to include the amplitude and duration effects of rupture directivity. Seismological Research Letters, 68(1), 199–222. https://doi.org/10.1785/gssrl.68.1.199

Stewart, J. P., & Seyhan, E. (2013). Semi-empirical nonlinear site amplification and its application in NEHRP site factors. In Berkeley, United States of America: Pacific Earthquake Engineering Research Center (Issue November).

Tepe, Ç., Sözbilir, H., Eski, S., Sümer, Ö., & Özkaymak, Ç. (2021). Updated historical earthquake catalog of region (western Anatolia) and its importance for the determination of seismogenic source. Turkish Journal of Earth Izmir Sciences, 30(8), Article 6. https://doi.org/10.3906/yer-2101-14

Tsai, C.-C., & Li, P.-C. (2024). Quantifying near-fault motion effects on soil liquefaction through effective stress site response analysis. Soil Dynamics and Earthquake Engineering, 183, 108779. https://doi.org/10.1016/j.soildyn.2024.108779

Tsai, C.-C., & Liu, H.-W. (2017). Site response analysis of vertical ground motion in consideration of soil nonlinearity. Soil Dynamics and Earthquake Engineering, 102, 124–136. https://doi.org/10.1016/j.soildyn.2017.08.024

Ministry of Environment and Urbanization. (2018). Turkish Building Earthquake Code (TEC 2018). Ankara, Turkey: Republic of Turkey, Ministry of Environment and Urbanization.

Turkish Ministry of Interior Disaster and Emergency Management Presidency (AFAD), Ankara, Turkiye, https://tadas.afad.gov.tr

Vucetic, M. and Dobry, R. (1991) Effect of Soil Plasticity on Cyclic Response. Journal of Geotechnical Engineering, 117, 89-107. http://dx.doi.org/10.1061/(ASCE)0733-9410(1991)117:1(89)

Zalachoris, G., & Rathje, E. M. (2015). Evaluation of one-dimensional site response techniques using borehole arrays. Journal of Geotechnical and Geoenvironmental Engineering, 141(8), 04015053. https://doi.org/10.1061/(ASCE)GT.1943-5606.0001366